[Research Paper] 대한금속·재료학회지 (*Korean J. Met. Mater.*), Vol. 56, No. 4 (2018) pp.272-279
DOI: 10.3365/KJMM.2018.56.4.272

High-temperature Corrosion of CrAlSiN Thin Films in N_2/0.1%H_2S Gas

Muhammad Ali Abro[1], Junhee Hahn[2], and Dong Bok Lee[3,*]

[1]*Department of Mechanical Engineering, MUET, SZAB Campus, Khairpur Mir's 66020, Pakistan*
[2]*Center for Energy Materials Metrology, Korea Research Institute of Standards and Science, Daejon 34113, Republic of Korea*
[3]*School of Advanced Materials Science & Engineering, Sungkyunkwan University, Suwon 16419, Republic of Korea*

Abstract: $Cr_{25.2}Al_{19.5}Si_{4.7}N_{50.5}$ thin films were deposited on steel substrates by cathodic arc plasma deposition. They consisted of alternating *fcc*-Cr(Al)N/*hcp*-Al(Cr,Si)N nanolayers. They were corroded at 900 and 1000 °C for 5-100 h in N_2/0.1%H_2S gas atmosphere. Their corrosion mechanism, the structure of the formed scales, and the role of film-constituting elements during corrosion were studied. Despite the presence of hydrogen and sulfur in the corrosion gas, the films displayed good corrosion resistance because Cr, Al, Fe preferentially reacted with impurity oxygen in the corrosion gas to form Cr_2O_3, Fe_3O_4, and amorphous Al_2O_3 owing to the thermodynamic stability of these oxides. The films were corroded by the outward diffusion of Cr, Al, Fe and nitrogen as well as the inward transport of sulfur and then oxygen. Silicon in the film was primarily oxidized by the inwardly transported oxygen. This study aimed to investigate the high-temperature corrosion behavior of nano-multilayered $Cr_{25.2}Al_{19.5}Si_{4.7}N_{50.5}$ thin films in a serious H_2S-containing environment.

(Received November 21, 2017; Accepted January 29, 2018)

Keywords: CrAlSiN thin film, H_2S corrosion, oxidation, sulfidation

1. INTRODUCTION

Hard chromium nitride (CrN) films are widely used to increase the service life of cutting tools, die molds, and machine components due to their high hardness, good adhesion to most substrates, and superior resistance to wear and oxidation. In order to further improve their mechanical properties and oxidation resistance, CrAlSiN films have been developed [1,2]. CrAlSiN films were synthesized by substituting smaller and oxidation-resistant elements such as Si and Al into the Cr sites of CrN films, which resulted in solution hardening with grain refinement [3] and precipitation of Si_3N_4 [4-6], leading to increased hardness [7], wear resistance [8-10], and thermal stability [3,4,11-13]. The good oxidation resistance of CrAlSiN films is attributed to the formation of protective oxides such as Cr_2O_3, Al_2O_3, and SiO_2 during oxidation at 800-1150 °C for 1-100 h in air [2,4,11,14,15].

H_2S is a harmful by-product of coal combustion, and synthetic gases produced in petrochemical plants, coal-gasification units, turbines, and heat exchangers. It can seriously deteriorate the corrosion resistance of metals by dissociating into sulfur and hydrogen. Accordingly, H_2S-corrosion is a major concern in petrochemical, fossil fuel-fired, gas-processing, and petroleum industries. Generally, sulfur forms non-protective, fast-growing sulfide scales while hydrogen migrates in metals interstitially, forming hydrogen clusters, embrittling metals, and greatly decreasing their high-temperature corrosion resistance [16,17]. To date, the high-temperature corrosion behavior of CrAlSiN films in H_2S-containing environments has not been adequately studied yet. Therefore, the objective of this study was to investigate the high-temperature corrosion behavior of nano-multilayered CrAlSiN films in H_2S-containing environments.

Nano-multilayered films have attracted a lot of interest due to their superior mechanical and lubrication properties in advanced tribological applications [8,10,13]. The film microstructure, corrosion products, and the corrosion mechanism of CrAlSiN films in N_2/0.1%H_2S-mixed gas were discussed in this study. The results of

*Corresponding Author: Dong Bok Lee
[Tel: +82-31-290-7355, E-mail: dlee@skku.ac.kr]

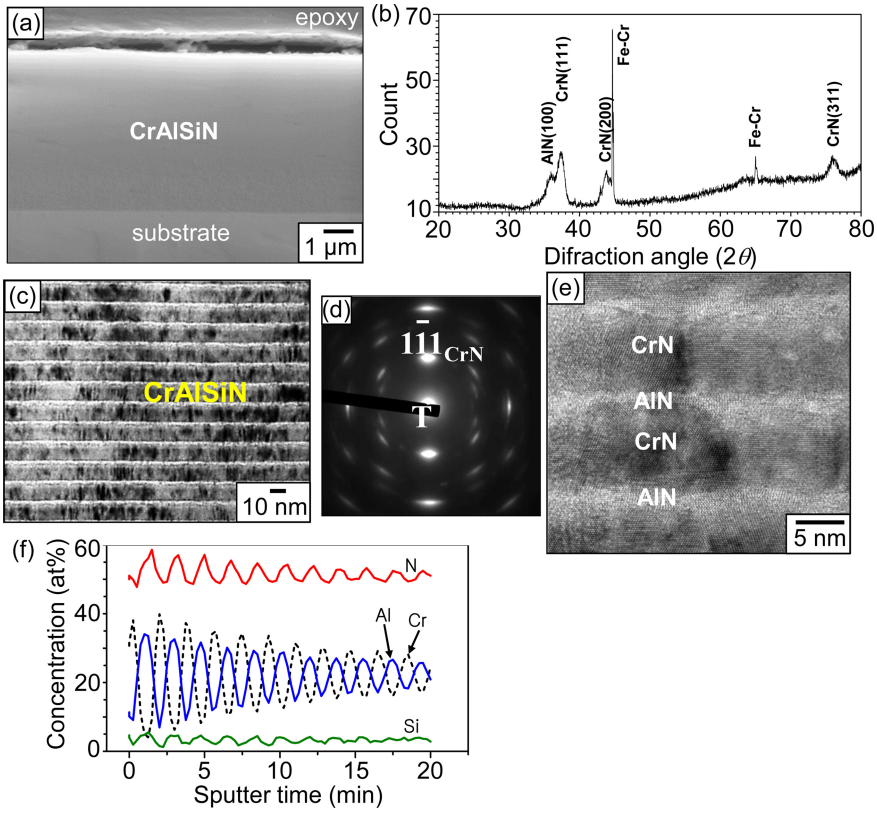

Fig. 1. CrAlSiN film deposited on steel. (a) SEM cross-sectional image, (b) XRD pattern, (c) TEM cross-sectional image, (d) selected area electron diffraction pattern of (c), (e) high-resolution TEM image of (c), (f) AES depth profiles from the film surface (sputtering rate = 18 nm/min for SiO_2).

this study will provide important information about the coating technique, which can protect metals from quite aggressive H_2S-containing environments.

2. EXPERIMENTAL

CrAlSiN films were deposited onto Fe-11.5 wt%Cr tool steel substrates to ~5 μm-thickness by cathodic arc plasma deposition under the following conditions: pressure, 4 Pa; temperature, 300 ºC; bias voltage, -100 V; $Al_{0.88}Si_{0.12}$ cathode arc current, 50 A; and Cr cathode arc current, 55A [1]. During deposition, the rotation speed of the substrates was set at 4.55 rpm, leading to the formation of nano-multilayered films with a composition of 25.2Cr-19.5Al-4.7Si-50.5N (at%), as determined by electron probe microanalysis (EPMA). Coated samples were placed into a quartz reaction tube centrally positioned in a furnace. They were corroded at 900 and 1000 ºC for 5-100 h under a flowing atmospheric N_2/0.1%H_2S-mixed gas (N_2 gas, 99.999% pure; H_2S gas, 99.5% pure). A thermogravimetric analyzer (TGA) could not be utilized to evaluate the corrosion kinetics because the corrosion gas was so aggressive that even the platinum inside the TGA was corroded considerably. The samples were subjected to EPMA. They were also analyzed using a scanning electron microscope (SEM), a high-powder X-ray diffractometer (XRD) with Cu-Kα radiation at 40 kV and 300 mA, an Auger electron spectrometer (AES), and a transmission electron microscope (TEM operated at 200 keV) equipped with EDS (5-nmϕ spot size). A TEM sample was prepared using a focused ion beam (FIB) system after carbon coating.

3. RESULTS AND DISCUSSION

The results of the SEM/XRD/TEM/AES analyses of the CrAlSiN films are shown in Fig. 1. A dense,

adherent film was deposited on the substrate (Fig. 1(a)). It consisted of *fcc*-CrN (JCPDS No. 76-2494) originating from the Cr target [6] and *hcp*-AlN (JCPDS No. 76-0702) originating from the $Al_{0.88}Si_{0.12}$ target (Fig. 1(b)). The intensity of the diffraction pattern of the Fe-Cr substrate (JCPDS No. 34-0396) was the strongest owing to the formation of a thin film. The low intensity of the film-constituting phases might have resulted from nano-multilayered film structure, as shown in Fig. 1(c). In this figure, *fcc*-CrN and *hcp*-AlN nanolayers are dark and white, respectively, according to their atomic contrast. The film exhibited a strong $(1\text{-}11)_{CrN}$ pattern (Fig. 1(d)). It is noted that (111) plane of the B1 type *fcc*-crystal structure had the lowest strain energy. Alternating CrN/AlN nanocrystalline multilayers were observed in Fig. 1(e). They were not pure but intermixed, as shown in Fig. 1(f). In particular, the Si tended to dissolve more in the AlN nanolayers than the CrN nanolayers. These results indicate that the CrAlSiN film consists of alternating *fcc*-Cr(Al)N/*hcp*-Al(Cr,Si)N nanolayers, displaying a preferred orientation along CrN(111).

Figure 2 shows the AES depth profiles of the CrAlSiN film corroded at 900 °C for 5 h. In order to find the corrosion mechanism of the film at an early stage, Au was sputter-deposited on the film prior to corrosion, and its depth profile was obtained after corrosion. The maximum concentration point of the inert Au marker indicates that sulfur and oxygen diffused inwardly while Cr, Al, and nitrogen diffused outwardly toward the surface. This led to the formation of the outermost Al_2O_3 scale dissolved with Cr, nitrogen, and sulfur. Silicon hardly existed in the outermost Al_2O_3 scale because of the inward diffusion of Si^{4+} ions [18]. Alumina formation in the N_2/0.1%H_2S-mixed gas might have occurred for the following reasons: (1) Al reacts preferentially with impurity oxygen in the corrosion gas because alumina is a highly stable oxide; (2) Oxides are generally more stable than corresponding sulfides; (3) Alumina will form in preference to chromia or silica because the former is thermodynamically more stable than the latter [19]. Like sulfur, hydrogen is expected to

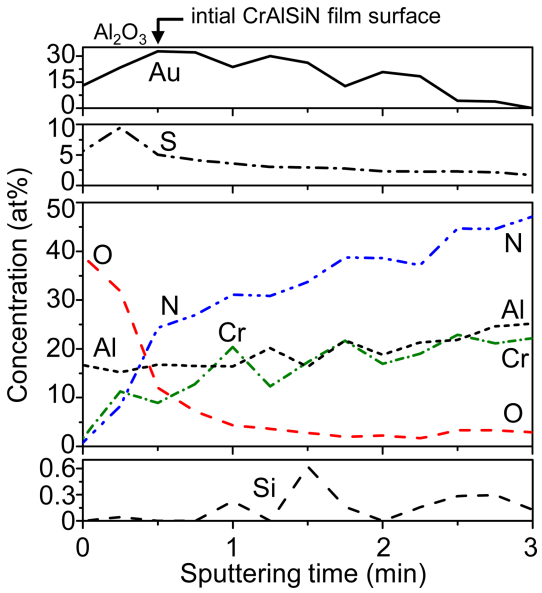

Fig. 2. AES depth profiles of CrAlSiN film after corrosion at 900 °C for 5 h (sputtering rate = 72 nm/min for SiO_2).

dissolve in the outermost Al_2O_3 scale. However, this was not confirmed due to the limitations of the analytical equipment utilized in the present study.

Figure 3 shows XRD/EPMA analytical results of the CrAlSiN film corroded at 900 °C for 100 h. In addition to *fcc*-CrN, *hcp*-AlN, and Fe-Cr substrates detected in Fig. 1(b), Cr_2N (JCPDS No. 79-2159) and Cr_2O_3 (JCPDS No. 85-0869) were also detected, as shown in Fig. 3(a). During corrosion, CrN, the major film phase, transformed partially to Cr_2N owing to nitrogen escape [13,20]. It was also partially oxidized to slowly growing Cr_2O_3 at the film surface. It is known that chromia grows primarily by the outward diffusion of Cr^{3+} ions along grain boundaries [21]. The film was oxidized to only a small extent, despite corrosion in serious H_2S-containing gas (Fig. 3(b)). The oxygen and sulfur maps shown in Fig. 3(c) indicate that the ingress of sulfur into the film was suppressed. In addition, oxidation overrode sulfidation. The Fe map indicates that Fe was able to diffuse out from the substrate into the film according to the concentration gradient. The superficial and extremely slowly growing Al_2O_3 scale depicted in Fig. 2 was hardly recognizable in the Al map shown in Fig. 3(c) because it was overgrown by the less stable but still

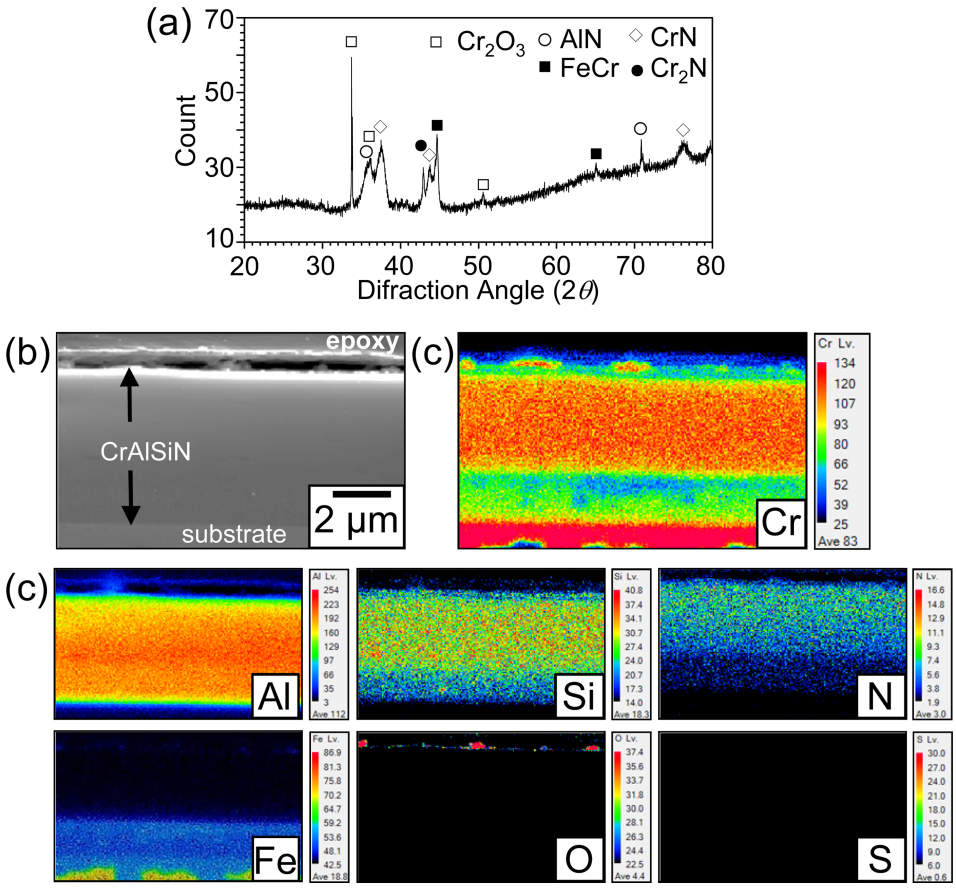

Fig. 3. CrAlSiN film after corrosion at 900 °C for 100 h. (a) XRD pattern, (b) EPMA cross-sectional image, (c) maps of (b).

protective Cr_2O_3 scale.

Figure 4 shows XRD/SEM/TEM/EDS analytical results of the CrAlSiN film corroded at 1000 °C for 20 h. The film constituting phases such as *hcp*-AlN and Cr_2N detected in Fig. 3(a) disappeared in Fig. 4(a) because the film corroded further. Corrosion products were Cr_2O_3 and Fe_3O_4 (Fig. 4(a)). These micrometer-sized oxide grains completely covered the surface (Fig. 4(b)). The scale was bi-layered (Fig. 4(c)). The outer scale was ~1 μm in thickness. It primarily consisted of Cr_2O_3 as the major phase and Fe_3O_4 as the minor phase (Figs. 4(a), 4(d), and 4(e)). Like Cr_2O_3, Fe_3O_4 grows by the outward migration of cations [16]. Cr_2O_3 and Fe_3O_4 coexisted (Fig. 4(a)). They were not pure, but intermixed as $(Cr,Fe)_2O_3$ and $(Fe,Cr)_3O_4$ (Fig. 4(d)). Figure 4(e) depicts an outer scale consisting of an outermost Fe_3O_4 grain followed by $(Cr,Fe)_2O_3$ grains and an inner scale consisting of tiny $(Al,Cr,Si)_2O_3$ grains. The inner Al_2O_3–rich scale was not detected in Fig. 4(a) primarily due to the formation of amorphous Al_2O_3. Its formation was facilitated by the preferential oxidation of Cr and Fe in the outer scale and the resultant depletion of Cr and Fe in the inner scale (Fig. 4(d)). Most of the Al and Si were oxidized in the inner scale, which consisted of fine oxide grains (Figs. 4(c)-(e)). However, a small amount of Al was able to diffuse outwardly to be dissolved in isostructural Cr_2O_3 in the outer scale, according to the TEM-EDS analysis. Such outward migration of Al is feasible because Al_2O_3 grows by the outward diffusion of cations as well as the inward diffusion of oxygen along grain boundaries [16]. The nanocrystalline nature of the film as shown in Fig. 1 might have facilitated the ingress of oxygen. Silicon was mostly oxidized in the inner scale owing to the high bonding energy of Si^{4+}-O^{2-} (465 kJ mol^{-1})

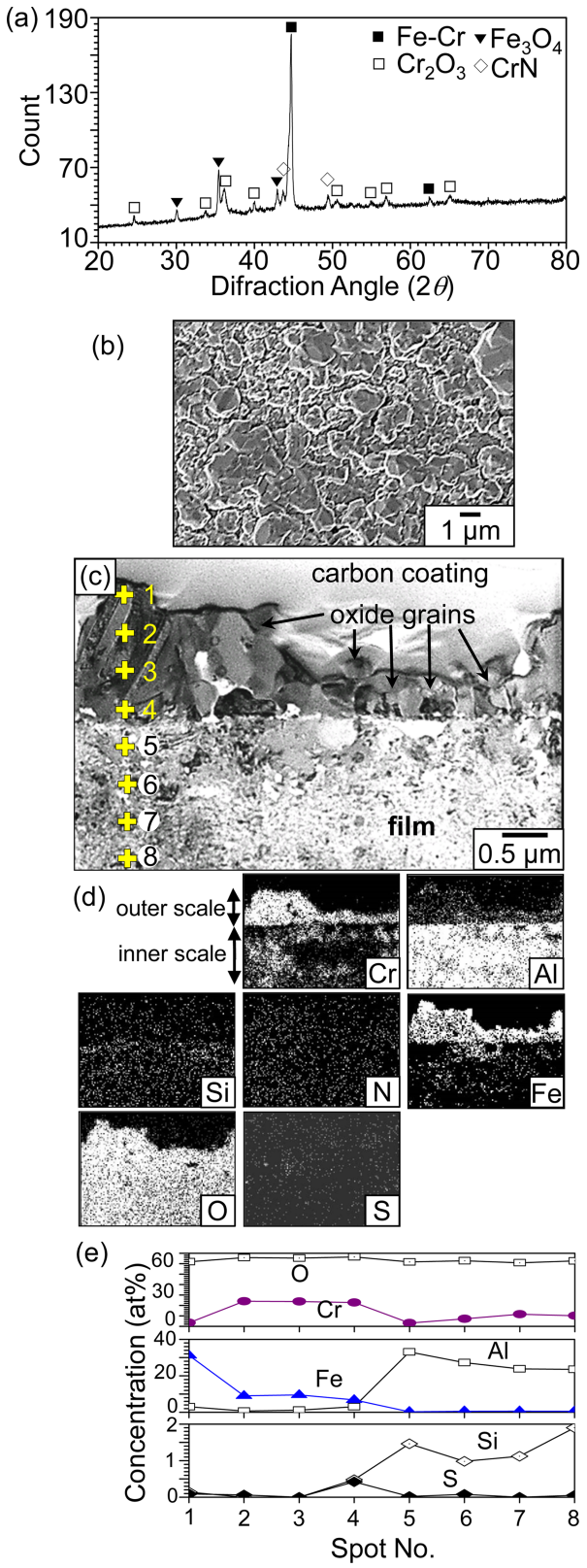

Fig. 4. CrAlSiN film after corrosion at 1000 °C for 20 h. (a) XRD pattern, (b) SEM top view, (c) TEM cross-sectional image, (d) EDS maps of (c), (e) EDS concentration profiles along spots 1-8 denoted in (c).

[22]. Taken together with the results shown in Fig. 3(c), the O and S maps shown in Fig. 4(e) clearly indicate that oxidation can override sulfidation, because oxides are thermodynamically more stable than corresponding sulfides [23]. Oxidation deprived the film of nitrogen and destroyed alternating nanolayers (Fig. 4(c)). The outer Cr_2O_3 and inner Al_2O_3 oxides could play an important role in protecting the film from harmful H_2S gas.

Figure 5 shows the XRD/EPMA analytical results of the CrAlSiN film corroded at 1000 °C for 50 h. Figure 5(a) displays a diffraction pattern similar to Fig. 4(a) except that CrN is no longer visible, owing to the increased corrosion time at 1000 °C. The scale shown in Fig. 5(b) grew to a thickness of ~2.3 μm. It primarily consisted of crystalline Cr_2O_3, Fe_3O_4, and amorphous Al_2O_3 (Fig. 5(c)). The outer scale and inner scale were rich in Cr and Al, respectively. Chromium diffused outwardly more than Al, leading to depletion of Cr or enrichment of Al underneath. This resulted in the formation of outer Cr_2O_3-rich Al_2O_3-containing scale and inner Al_2O_3-rich Cr_2O_3-containing scale. Iron continuously diffused from the substrate toward the surface, forming Fe_3O_4. The accumulation of Si around the interface of the inner oxide scale and the uncorroded film was mainly

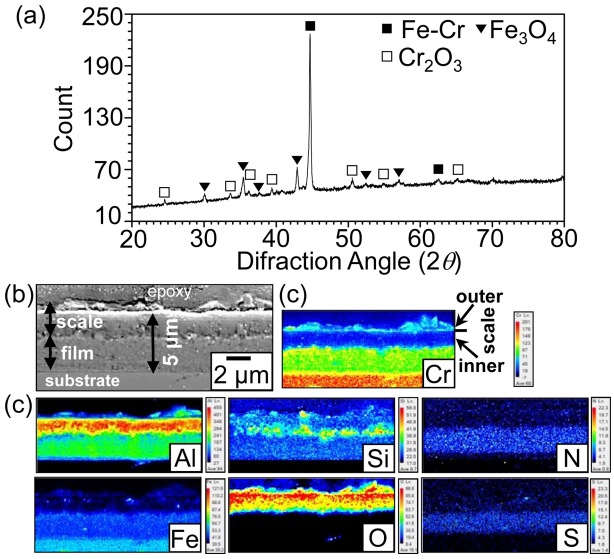

Fig. 5. CrAlSiN film after corrosion at 1000 °C for 50 h. (a) XRD pattern, (b) EPMA cross-sectional image, (c) maps of (b).

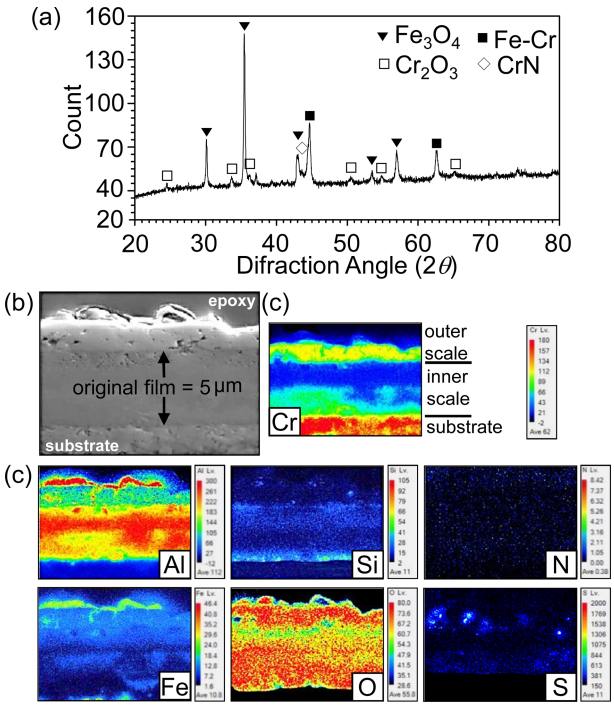

Fig. 6. CrAlSiN film after corrosion at 1000 °C for 100 h. (a) XRD pattern, (b) EPMA cross-sectional image, (c) maps of (b).

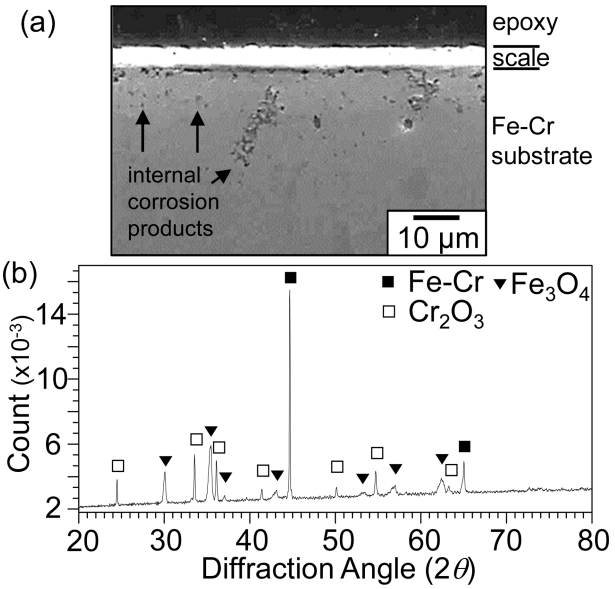

Fig. 7. Fe-11.5 wt%Cr steel substrate after corrosion at 900 °C for 5 h. (a) SEM cross-sectional image, (b) XRD pattern.

attributed to the relative thermodynamic nobility of Si. However, silica was undetected in Fig. 5(a) due to its amorphous structure. Nitrogen in the uncorroded film was still recognizable (Fig. 5(c)). Grain boundaries of fine oxides would provide an easy diffusion path for sulfur. The solubility of sulfur in most oxides is very limited [24]. Therefore, more sulfur was present in the film than in the oxide scale.

The XRD/EPMA results of the CrAlSiN film in the final stage of corrosion are shown in Fig. 6. Fe_3O_4 was the major oxide while Cr_2O_3 was the minor oxide (Fig. 6(a)). Here, amorphous Al_2O_3 was undetected. The film was almost completely corroded (Figs. 6(b-c)). Based on the original film thickness of ~5 μm and the distribution of Si as a marker [25], the original film surface could be identified. This allowed the outer and inner scales to be differentiated, as denoted in the Cr map shown in Fig. 6(c). The enrichment of Cr in the outer scale with a thickness of ~2 μm depleted Cr in the upper part of the inner scale. Al and Fe diffused outwardly up to the outermost scale (Fig. 6(c)). The outward transport of Si was indistinct because Si was partially expelled from the growing oxide scale owing to its nobility. Silicon existed more in the inner scale than the outer scale. Nitrogen that existed in the uncorroded film (*see* the N map shown in Fig. 5(c)) was almost completely liberated from the film as the oxidation progressed (*see* the N map shown in Fig. 6(c)). Nitrogen in the N_2/0.1%H_2S-mixed gas was not able to penetrate the oxide layer due mainly to the negligible solubility of nitrogen in Cr_2O_3 [26]. In this study, corrosion was inevitably dominated by oxidation rather than sulfidation.

Figure 7 shows the SEM/XRD analytical results of the Fe-11.5 wt%Cr substrate that was corroded under the same corrosion conditions given in Fig. 2. The scale was ~7 μm-thick, underneath which internal corrosion occurred up to ~25 μm in depth (Fig. 7(a)). It consisted of Fe_3O_4 and Cr_2O_3 (Fig. 7(b)). These oxides were similarly detected in the XRD patterns shown in Figs. 4-6. However, the thickness of the scale outlined in Fig. 2 was estimated to be ~40 nm based on the sputtering rate. Clearly, the CrAlSiN film showed superior corrosion resistance, even in hostile H_2S-environments.

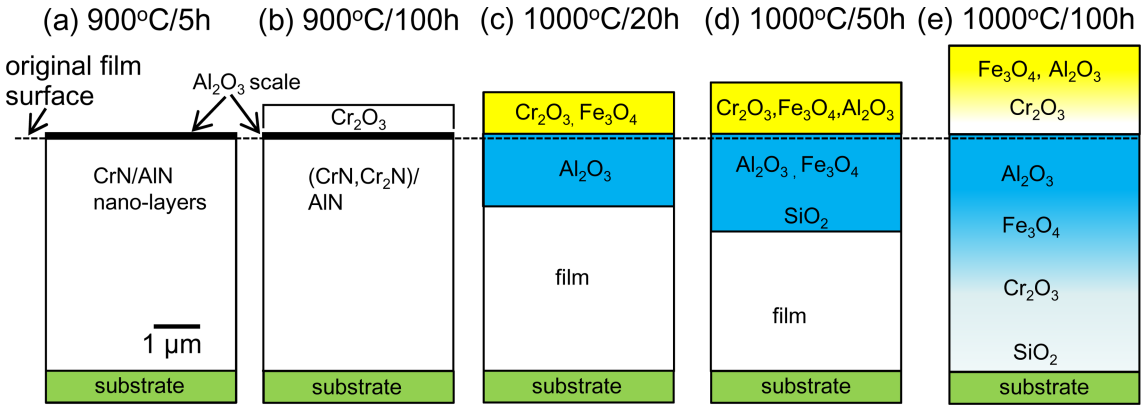

Fig. 8. Schematic morphology of scales formed on the CrAlSiN film during corrosion.

4. CONCLUSIONS

$Cr_{25.2}Al_{19.5}Si_{4.7}N_{50.5}$ thin films consisted of alternating *fcc*-CrN/*hcp*-AlN nanolayers, where Al, Cr, and Si were intermixed. Their corrosion at 900-1000 °C in N_2/ 0.1%H_2S-mixed gas was governed by the outward diffusion of Al, Cr, and Fe ions, together with the inward diffusion of S and O ions. Scale morphology kept changing as corrosion progressed, as shown in Fig. 8. In the early stage, a superficial and highly stable Al_2O_3 film was formed by the preferential oxidation of Al (Fig. 8(a)). Soon, it was overgrown by less stable Cr_2O_3 due to the outward diffusion of Cr (Fig. 8(b)). Later, the increased outward diffusion of Cr and Fe resulted in the formation of an outer scale rich in $(Cr,Fe)_2O_3$ and $(Fe,Cr)_3O_4$, which facilitated the formation of an inner scale rich in amorphous Al_2O_3 (Fig. 8(c)). As corrosion progressed, Al also noticeably diffused outwardly, besides Cr and Fe. The outer scale then became rich in Cr_2O_3, Fe_3O_4, and Al_2O_3, which favored the formation of an inner scale rich in Fe_3O_4 and amorphous Al_2O_3 (Fig. 8(d)). Unlike Cr, Al, and Fe, silicon tended to be oxidized around the scale/film interface owing to its nobility (Fig. 8(d)). Eventually, the film corroded to the outer (Cr_2O_3, Fe_3O_4, Al_2O_3)-rich scale and inner (Al_2O_3, Fe_3O_4, SiO_2, Cr_2O_3)-rich scale (Fig. 8(e)). At this stage, Fe and Al were able to diffuse up to the outermost surface to a certain extent while SiO_2 kept accumulating at the bottom of the scale. The $Cr_{25.2}Al_{19.5}Si_{4.7}N_{50.5}$ thin films displayed good corrosion resistance even in an H_2S–containing environment owing to prevailing oxidation.

ACKNOWLEDGMENT

This work was supported by the project “Development of the High-Efficiency Low-Emission Future Energy Production Technology (EO15580)” of National Research Council of Science & Technology (NST) grant by the Korea Government (MSIP) (No. CRC-15-07-KIER).

REFERENCES

1. S. K. Kim, V. V. Le, P. V. Vinh, and J. W. Lee, *Surf. Coat. Technol*. **202**, 5400 (2008).
2. D. B. Lee, T. D. Nguyen, and S. K. Kim, *Surf. Coat. Technol*. **203**, 1199 (2009).
3. C. B. Liu, W. Pei, F. Huang, and L. Chen, *Vacuum* **125**, 180 (2016).
4. S. K. Tien, C. H. Lin, Y. Z. Tsai, and J. G. Duh, *Surf. Coat. Technol*. **202**, 735 (2007).
5. J. L. Endrino, S. Palacín, M. H. Aguirre, A. Gutiérrez, and F. Schäfers, *Acta Mater*. **55**, 2129 (2007).
6. H. W. Chen, Y. C. Chan, J. W. Lee, and J. G. Duh, *Surf. Coat. Technol*. **205**, 1189 (2010).
7. Y. X. Wang, S. Zhang, J. W. Lee, W. S. Lew, D. Sun, and B. Li, *Surf. Coat. Technol*. **231**, 346 (2013).
8. Y. Y. Chang and H. M. Lai, *Surf. Coat. Technol*. **259**, 152 (2014).

9. C. C. Chang, H. W. Chen, J. W. Lee, and J. G. Duh, *Surf. Coat. Technol*. **284**, 273 (2015).
10. V. C. Teles, J. D. B. de Mello, and W. M. da Silva Jr, *Wear* **376-377**, 1691 (2017).
11. Y. Y Chang, C. P. Chang, D. Y. Wang, S. M. Yang, and W. Wu, *J. Alloy. Compd*. **461**, 336 (2008).
12. S. Zhang, L. Wang, Q. Wang, and M. Li, *Surf. Coat. Technol*. **214**, 153 (2013).
13. L. He, L. Chen, and Y. Xu, *Mater. Charact*. **125**, 1 (2017).
14. Y. Y. Chang and C. Y. Hsiao, *Surf. Coat. Technol*. **204**, 992 (2009).
15. H. W. Chen, Y. C. Chan, J. W. Lee, and J. G. Duh, *Surf. Coat. Technol*. **206**, 1571 (2011).
16. N. Birks, G. H. Meier, and F. S. Pettit, *Introduction to the High-Temperature Oxidation of Metals, 2nd ed.,* pp.63-168, Cambridge University Press, England (2006).
17. P. Y.adav and D. B. Lee, *Met. Mater. Int*. **23**, 896 (2017).
18. P. Kofstad, *Oxid. Met*. **44**, 3 (1995).
19. I. Barin, *Thermochemical Data of Pure Substances*, VCH, Germany (1989).
20. T. Polcar and A. Cavaleiro, *Surf. Coat. Technol*. **206**, 1244 (2011).
21. G. Simkovich, *Oxid. Met*. **44**, 501 (1995).
22. M. A. Schiavon, S. U. A. Redondo, S. R. O. Pina, and I. V. P. Yoshida, *J. Non-Cryst. Solids* **304**, 92 (2002).
23. P. Yadav, S. C. Kwon, Y. Lin, S. Zhang, and D. B. Lee, *Korean J. Met. Mater*. **55**, 222 (2017)
24. H. J. Grabke, *High Temperature Corrosion in Complex, Multi-reactant Gaseous Environments*. In *High Temperature Materials Corrosion in Coal Gasification Atmospheres*, (ed. J. F. Norton), pp.59-82, Elsevier Applied Science Publishers, England (1984).
25. D. B. Lee and S. W. Park, *Oxid. Met.* **67**, 51 (2007).
26. D. J. Young, *High Temperature Oxidation and Corrosion of Metals*, p.174, Elsevier Science, England (2008).